ResearchGate

See discussions, stats, and author profiles for this publication at: https://www.researchgate.net/publication/231339347

Structural characterization of low-spin iron(III) complexes of octaethyloxoporphyrin. Inorg Chem

ARTICLE *in* INORGANIC CHEMISTRY · JUNE 1993

Impact Factor: 4.76 · DOI: 10.1021/ic00065a017

CITATIONS
31

READS
13

3 AUTHORS, INCLUDING:

Alan Balch
University of California, Davis
597 PUBLICATIONS **18,708** CITATIONS
SEE PROFILE

Bruce C Noll
Bruker AXS Inc.
286 PUBLICATIONS **6,644** CITATIONS
SEE PROFILE

Available from: Alan Balch
Retrieved on: 16 January 2016

Structural Characterization of Low-Spin Iron(III) Complexes of Octaethyloxoporphyrin

Alan L. Balch,* Bruce C. Noll, and Nasser Safari

Department of Chemistry, University of California, Davis, California 95616

Received December 17, 1992

Low-spin ($S = {}^1/_2$), six-coordinate iron(III) complexes of the octaethyloxoporphyrin anion (OEOP) have been obtained by treating high-spin ($S = {}^5/_2$), six-coordinate (OEOP)$Fe^{III}Cl_2$ with strong-field ligands. These nucleophiles do not attack the oxoporphyrin ligand, which remains intact. The cyano complex (OEOP)$Fe^{III}(CN)_2 \cdot 1.6CH_2Cl_2$ has been isolated and studied by X-ray crystallography. It crystallizes in the monoclinic space group $P2_1/c$ with $a = 12.750(4)$ Å, $b = 8.069(3)$ Å, $c = 19.728(8)$ Å, and $\beta = 99.67(3)°$ at 130 K with $Z = 2$. Refinement of 1250 reflections with $F > 6.0\sigma(F)$ and 123 parameters yields $R = 0.076$, $R_w = 0.078$. The complex is centrosymmetric with the six-coordinate iron located at the center of symmetry. Hence, there is disorder in the location of the meso-oxygen atom. The Fe–N distances are 1.976(9) and 1.955(9) Å. The magnetic moment (2.4 μ_B at 20 °C in dichloromethane) and ESR spectrum (g = 2.4, 2.2, 1.8) confirm the low-spin formulation. The ^1H NMR spectrum has been analyzed by one- and two-dimensional studies. Stepwise binding of 4-methylimidazole (4-MeIm, which coordinates as 5-MeIm) has been followed by ^1H NMR measurements at –60 °C. Evidence for the successive formation of two low-spin species, $[(OEOP)Fe(5\text{-}MeIm)Cl]^+$ and $[(OEOP)Fe(5\text{-}MeIm)_2]^{2+}$, is presented. Addition of excess amounts of these strong-field ligands results in the reduction of Fe^{III} to Fe^{II}.

Introduction

Catabolism of heme produces bilirubin. As shown in Scheme I, two enzymes, heme oxygenase and biliverdin reductase, are involved. The first of these, heme oxygenase, utilizes dioxygen to carry out a regiospecific cleavage of the heme macrocycle at the α-methine position.[1-3] It releases carbon monoxide and iron to give biliverdin. The second enzyme, biliverdin reductase, converts biliverdin to bilirubin.

Oxidation of heme in pyridine by dioxygen in the presence of an electron donor such as ascorbate, which is termed coupled oxidation, has been extensively studied as a model for heme degradation.[4-18] Studies of the mechanism of heme breakdown suggest that enzymatically mediated heme cleavage may be similar to coupled oxidation.[1] Oxidation of heme in model systems produces a green intermediate called verdohemochrome. On hydrolysis, verdohemochrome can be transformed to biliverdin. Verdohemochrome is generally isolated in less than 50% yield.[11-18]

Recent structural studies from this laboratory[18] have confirmed the notion that verdohemochrome and its derivatives contain the oxoporphyrin ligand A. A combination of ^1H NMR and X-ray diffraction studies established the interrelations of the verdoheme derivatives shown in Scheme II. Here we are concerned with further chemistry of the high-spin, six-coordinate complex **3** and specifically with the effects altering the axial ligands in this complex. The oxoporphyrin macrocycle is sensitive to some nucleophiles. Attack by hydroxide or hydrogen peroxide has been shown to cause ring opening with the formation of biliverdin derivatives.[12] Thus it is a matter of interest to see whether the axial ligation of iron in **3** can be altered without having the oxoporphyrin suffer nucleophilic attack.

Scheme I

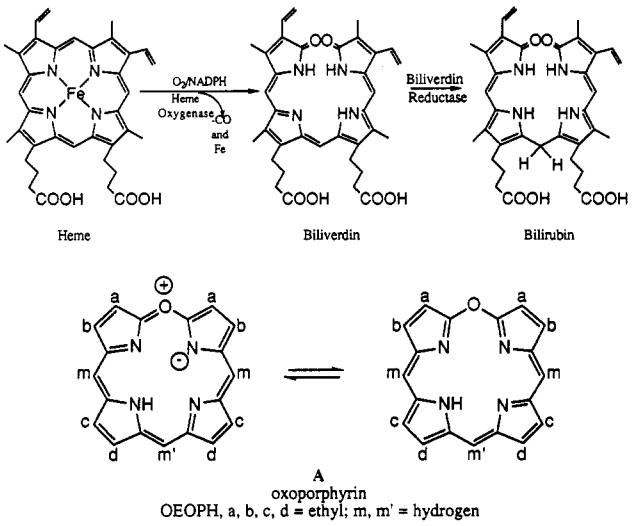

Results

Formation and Characterization of (OEOP)$Fe^{III}(CN)_2$. Treatment of a green dichloromethane solution of (OEOP)$Fe^{III}Cl_2$ with 2 equivalents of bis(triphenylphosphine)nitrogen(1+) cyanide produces a blue solution from which dark red crystals of (OEOP)$Fe^{III}(CN)_2$ were obtained by precipitation with diethyl ether. The air-stable product is soluble in dichloromethane and chloroform to form blue solutions, but it is insoluble in methanol or diethyl ether.

(1) Bissell, D. M. In *Liver: Heme Catabolism and Bilirubin Formation*; Ostrow, J. D., Ed.; Marcel Dekker Inc.: New York, 1986; Vol. 5, p 133.
(2) Schmid, R.; McDonagh, A. F. In *The Porphyrins*, Dolphin, D., Ed.; Academic Press: New York, 1979; Vol. 6, p 258.
(3) O'Cara, P. In *Porphyrins and Metalloporphyrins*; Smith, K. M., Ed.; Elsevier: New York, 1975; p 122.
(4) Warburg, O.; Negelein, E. *Chem. Ber.* **1930**, *63*, 1816.
(5) Foulkes, E. C.; Lemberg, R.; Pardonn, P. *Proc. R. Soc. London* **1951**, *B138*, 386.
(6) Lemberg, R. *Rev. Pure Appl. Chem.* **1956**, *6*, 1.
(7) Levin, E. Y. *Biochemistry* **1966**, *5*, 2845.
(8) Jackson, A. H.; Kenner, G. W.; Smith, K. M. *J. Chem. Soc.* **1968**, 302.
(9) Bonnett, R.; Dimsdale, M. J. *J. Chem. Soc. Soc., Perkin Trans. 1* **1972**, *79*, 1393.
(10) Saito, S.; Itano, H. A. *Proc. Natl. Acad. Sci. U.S.A.* **1982**, *79*, 1393.
(11) Lagarias, J. C. *Biochem. Biophys. Acta* **1982**, *717*, 12.
(12) Itano, H. A.; Hirota, T. *Tetrahedron Lett.* **1983**, *24*, 995.
(13) Sano, S.; Sano, T.; Morishima, I.; Shiro, Y.; Maeda, Y. *Proc. Natl. Acad. Sci. U.S.A.* **1986**, 531.
(14) Saito, S.; Itano, H. A. *J. Chem. Soc., Perkin Trans.* **1986**, 1.
(15) Masuoka, N.; Itano, H. A. *Biochemistry* **1987**, *26*, 3672.
(16) Saito, S.; Sumita, S.; Iwai, K.; Sano, H. *Bull. Chem. Soc. Jpn.* **1988**, *61*, 3539.
(17) Modi, S.; Behere, D. V.; Shedbalkar, V. P. *J. Chem. Res.* **1988**, 244.
(18) Balch, A. L.; Latos-Grażyński, L.; Noll, B. C.; Olmstead, M. M.; Szterenberg, L.; Safari, N. *J. Am. Chem. Soc.* **1993**, *115*, 1422.

0020-1669/93/1332-2901$04.00/0 © 1993 American Chemical Society

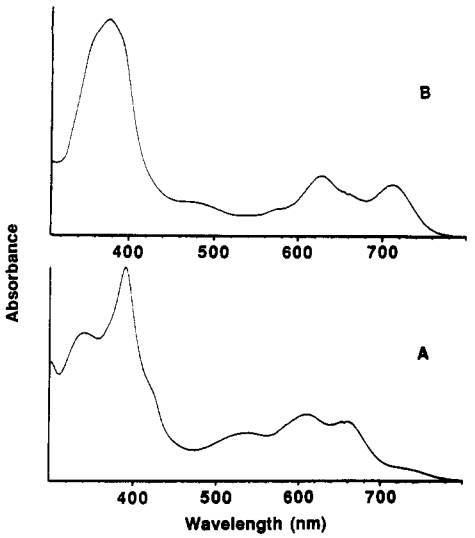

Figure 1. UV/vis absorption spectra of chloroform solutions of (A) (OEOP)$Fe^{III}(CN)_2$ and (B) (OEOP)$Fe^{III}Cl$.

Scheme II

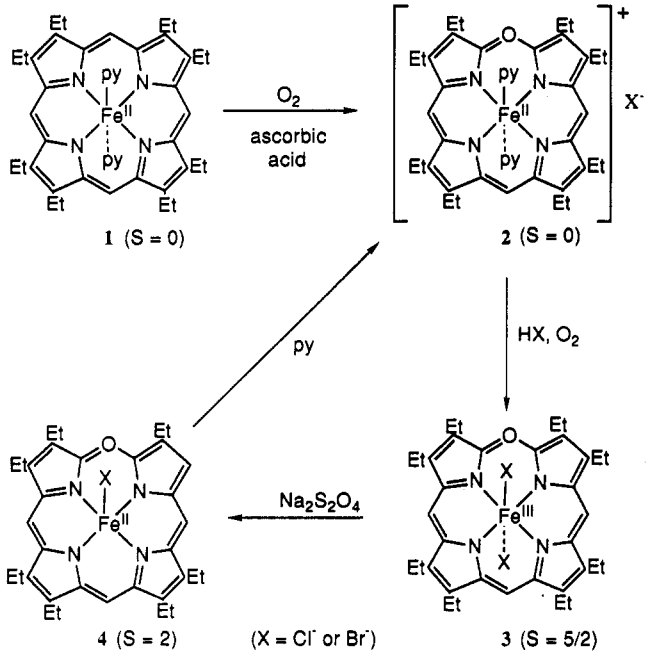

The electronic absorption spectrum of (OEOP)$Fe^{III}(CN)_2$ is shown in Figure 1, trace A, where it is compared to that of the precursor, (OEOP)$Fe^{III}Cl_2$, in trace B. Exchange of cyanide for chloride produces significant changes in the Soret absorption and also in the 550–750 nm region.

The low-spin ($S = {}^1/_2$) nature of (OEOP)$Fe^{III}(CN)_2$ has been established by magnetic susceptibility and ESR spectral measurements. The magnetic moment of (OEOP)$Fe^{III}(CN)_2$ in dichloromethane solution at 20 °C is 2.4(2) μ_B. The electron spin resonance spectrum of the complex (in a frozen dichloromethane solution at 6 K) shows a typical low-spin pattern[19] with g = 2.4, 2.2, and 1.8.

The ^{1}H NMR spectrum of (OEOP)$Fe^{III}(CN)_2$ in chloroform-*d* is shown in Figure 2. Trace A shows the normal spectrum, while trace B shows an inversion recovery spectrum in which the resonances of diamagnetic material are inverted or decreased in intensity. The resonance assignments can be readily made on the basis of relative integrated intensities. The two resonances

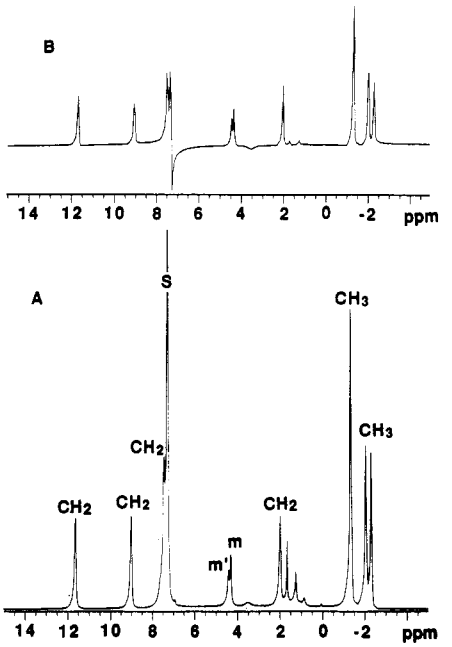

Figure 2. 300-MHz ^{1}H NMR spectrum of (OEOP)$Fe^{III}(CN)_2$ in chloroform-*d* solution at 19.3 °C (A). Resonance labels: m, m′ = meso protons; CH_2 = methylene protons; CH_3 = methyl protons. Inset B shows a T_1 inversion recovery spectrum that was obtained using a 50-ms delay.

at 4.5 and 4.4 ppm result from the two types of meso protons. The four equally intense resonances at 11.6, 9.1, 7.4, and 1.9 ppm are due to the methylene protons. The fact that only four methylene resonances are seen indicates that the complex possesses identical ligation on either side of the porphyrin plane. The three resonances at high field are assigned to the methyl protons. Two-dimensional magnitude COSY (M-COSY) experiments are effective as assignment strategies for paramagnetic iron porphyrins and their derivatives.[20] Figure 3 shows the M-COSY plot that was obtained from a chloroform solution of (OEOP)$Fe^{III}(CN)_2$ at 20 °C. A normal spectrum appears at the top. This spectrum confirms the assignment of methyl and methylene resonances that was made on the basis of intensities, since a single cross peak connects resonances of the methyl and the methylene protons within any one ethyl group.

Figure 4 shows a plot of chemical shift versus $1/T$ for the resonances of (OEOP)$Fe^{III}(CN)_2$. The linearity of these plots indicates that the complex obeys the Curie law, as expected for a simple, low-spin formulation.

Crystal and Molecular Structure of (OEOP)$Fe^{III}(CN)_2$·1.6CH_2Cl_2. This compound crystallized with one-half of the oxoporphyrin complex and eight-tenths of a disordered dichloromethane molecule in the asymmetric unit. A drawing of the oxoporphyrin complex is shown in Figure 5. Atomic positional parameters are given in Table I. Table II gives a listing of important bond distances and angles.

The iron ion is located on a crystallographic inversion center. As a consequence, the molecule is disordered with the oxygen atom, O(1), and the meso carbon C(1) occupying the same site. These two atoms were refined as coincident with a site occupancy of 50% for each. There does not appear to be any disorder involving the other meso carbon, C(6). The thermal parameter of C(6) is not abnormal and is equal to those of the two adjacent carbon atoms, C(5) and C(7). The protons attached to C(6) and to C(1) were identified in a difference electron density map. The ratio of electron densities for the peak associated with C(6) to that associated with C(1) is 1.7:1. Ideally that ratio should be 2:1.

(19) Palmer, G. In *The Porphyrins*; Dolphin, D., Ed.; Academic Press: New York, 1979; Vol. IV, p 313.

(20) Keating, K. A.; de Ropp, J. S.; La Mar, G. N.; Balch, A. L.; Shiau, F.-Y.; Smith, K. M. *Inorg. Chem.* **1991**, *30*, 3258.

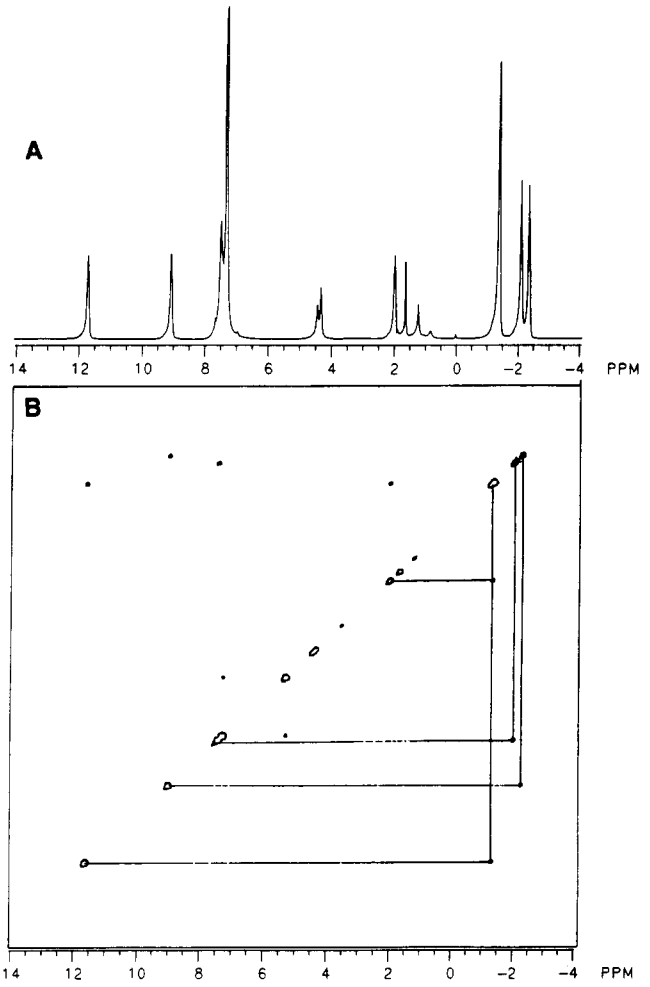

Figure 3. ^{1}H NMR M-COSY spectrum of (OEOP)Fe^{III}(CN)$_2$ in chloroform-*d* solution at 20 °C. A normal spectrum is shown at the top. Cross peaks between resonances of the four distinct ethyl groups are connected below the diagonal.

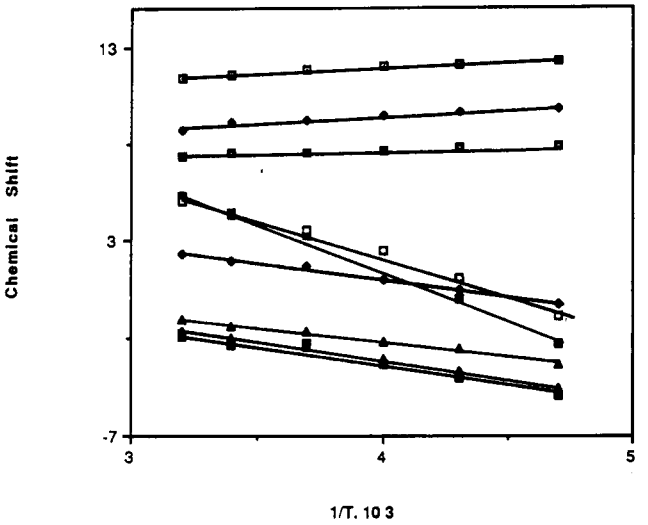

Figure 4. Chemical shift versus T^{-1} for the protons in (OEOP)Fe^{III}(CN)$_2$.

The iron has six-coordinate geometry. Its structural features are consistent with structural parameters observed for low-spin, six-coordinate iron(III) porphyrins.[21,22] The Fe–N distances (1.976(9), 1.955(9) Å) are at the short end of the range (1.970–2.000 Å) found for analogous porphyrin complexes.[21,22] This is consistent with the notion that the macrocyclic cavity in the oxoporphyrin is just slightly smaller than that in a porphyrin. The Fe–C distance in (OEOP)Fe^{III}(CN)$_2$ is 1.969(10) Å, which is comparable to the Fe–C distance of 1.975 Å in [(TPP)-Fe(CN)$_2$]$^-$.[23] The Fe–C–N angle (177.4(11)°) is nearly linear, while the C–Fe–C angle is crystallographically required to be linear. The oxoporphyrin skeleton is nearly planar. This can be best appreciated by examining Figure 6, which shows the out-of-plane displacements (in units of 0.01 Å) for each atom within the macrocycle's core.

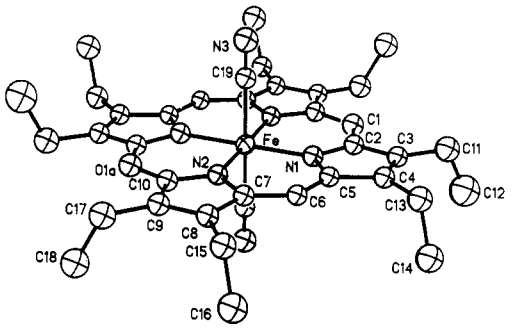

Figure 5. Perspective view of (OEOP)Fe^{III}(CN)$_2$ with 50% thermal contours for all atoms.

Table I. Atomic Coordinates (×10^4) and Equivalent Isotropic Displacement Coefficients (Å^2 × 10^3) for (OEOP)Fe^{III}(CN)$_2$·1.6CH$_2$Cl$_2$

	x	*y*	*z*	*U*(eq)
Fe	0	0	0	31(1)
N(1)	1201(7)	1548(12)	0(4)	32(2)
N(2)	−640(6)	1505(12)	592(4)	29(2)
N(3)	−1215(7)	1848(14)	−1269(5)	44(3)
Cl(1)	4519(10)	30(28)	1981(7)	54(4)
Cl(1A)	4503(8)	150(20)	1709(6)	65(3)
Cl(1B)	4034(22)	277(45)	1327(14)	81(8)
Cl(2)	2677(10)	1967(18)	2223(7)	52(4)
Cl(2A)	3052(12)	2091(18)	2418(6)	41(3)
Cl(2B)	3545(15)	1923(25)	2518(8)	47(4)
O(1)	2219(6)	19(15)	−700(4)	39(2)
C(1)	2219(6)	19(15)	−700(4)	39(2)
C(2)	2053(8)	1364(16)	−333(5)	31(2)
C(3)	2727(9)	2769(16)	−237(5)	32(3)
C(4)	2292(8)	3874(16)	167(5)	32(3)
C(5)	1332(8)	3101(15)	308(5)	28(2)
C(6)	648(8)	3751(15)	693(5)	28(2)
C(7)	−266(8)	3054(15)	843(5)	29(2)
C(8)	−986(8)	3809(16)	1244(5)	32(3)
C(9)	−1809(9)	2724(16)	1219(5)	33(3)
C(10)	−1577(8)	1322(16)	831(5)	31(2)
C(11)	3743(9)	2899(19)	−526(6)	48(3)
C(12)	4692(11)	2269(21)	−58(8)	76(5)
C(13)	2725(9)	5505(15)	420(5)	42(3)
C(14)	3389(9)	5441(18)	1134(5)	52(3)
C(15)	−809(8)	5430(15)	1612(5)	40(3)
C(16)	−127(9)	5216(19)	2316(5)	53(3)
C(17)	−2814(9)	2913(18)	1539(6)	45(3)
C(18)	−2795(10)	1828(18)	2188(6)	53(3)
C(19)	−772(8)	1142(16)	−816(5)	33(3)
C(20)	3176(13)	797(24)	1726(8)	60(5)

Reaction of (OEOP)Fe^{III}Cl$_2$ with 4-Methylimidazole. This reaction has been monitored at −60 °C by ^{1}H NMR spectroscopy. At this temperature, the spectrum has enhanced dispersion, and the resonances can be readily identified. When coordinated, 4-methylimidazole (4-MeIm) binds as 5-methylimidazole (5-MeIm), B.[24] The results of adding 4-MeIm to (OEOP)Fe^{III}Cl$_2$ in chloroform solution are shown in Figure 7. Trace A shows the ^{1}H NMR spectrum after the addition of 1 equiv of 4-MeIm, while trace C shows the spectrum after the addition of 2.3 equiv of 4-MeIm. Trace C was obtained under inversion recovery

(21) Scheidt, W. R.; Reed, C. A. *Chem. Rev.* **1981**, *81*, 543.
(22) Scheidt, W. R.; Lee, Y. J. *Struct. Bonding* **1987**, *64*, 1.
(23) Scheidt, W. R.; Maller, K. J.; Matano, K. J. *J. Am. Chem. Soc.* **1980**, *102*, 2017.
(24) Satterlee, J. D.; LaMar, G. N. *J. Am. Chem. Soc.* **1976**, *98*, 2804.

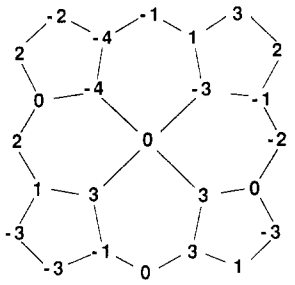

Figure 6. Diagram of the oxoporphyrin core. Each atom symbol has been replaced by a number that represents the perpendicular displacement (in units of 0.01 Å) of that atom from the mean plane of the oxoporphyrin.

Table II. Bond Lengths (Å) and Angles (deg) for $(OEOP)Fe^{III}(CN)_2$

	Bond Lengths		
Fe–N(1)	1.976(9)	Fe–N(2)	1.955(9)
Fe–C(19)	1.969(10)	Fe–C(19A)	1.969(10)
N(1)–C(2)	1.369(14)	N(1)–C(5)	1.391(15)
N(2)–C(7)	1.399(15)	N(2)–C(10)	1.365(14)
N(3)–C(19)	1.128(14)	O(1)–C(2)	1.341(16)
O(1)–C(10A)	1.356(16)	C(1)–C(2)	1.341(16)
C(1)–C(10A)	1.356(16)	C(2)–C(3)	1.416(17)
C(3)–C(4)	1.373(17)	C(6)–C(7)	1.371(15)
C(4)–C(5)	1.442(16)	C(8)–C(9)	1.362(16)
C(5)–C(6)	1.353(15)	C(9)–C(10)	1.425(17)
C(7)–C(8)	1.442(16)		
	Bond Angles		
N(1)–Fe–N(2)	90.5(4)	N(1)–Fe–C(19)	89.1(4)
N(2)–Fe–C(19)	89.8(4)	N(1)–Fe–N(1A)	180.0(1)
N(2)–Fe–N(1A)	89.5(4)	N(2)–Fe–N(2A)	180.0(1)
N(1)–Fe–C(19A)	90.9(4)	N(2)–Fe–C(19A)	90.2(4)
C(19)–Fe–C(19A)	180.0(1)	Fe–N(1)–C(2)	127.5(8)
Fe–N(1)–C(5)	127.3(7)	C(2)–N(1)–C(5)	105.1(9)
Fe–N(2)–C(7)	128.0(7)	Fe–N(2)–C(10)	128.1(8)
C(7)–N(2)–C(10)	103.9(9)	C(2)–O(1)–C(10A)	127.2(9)
C(2)–C(1)–C(10A)	127.2(9)	N(1)–C(2)–O(1)	123.8(10)
N(1)–C(2)–C(1)	123.8(10)	N(1)–C(2)–C(3)	111.2(10)
O(1)–C(2)–C(3)	124.9(10)	C(1)–C(2)–C(3)	124.9(10)
C(2)–C(3)–C(4)	107.6(10)	C(3)–C(4)–C(5)	105.7(10)
N(1)–C(5)–C(4)	110.4(9)	N(1)–C(5)–C(6)	123.5(10)
C(4)–C(5)–C(6)	126.0(11)	C(5)–C(6)–C(7)	127.9(11)
N(2)–C(7)–C(6)	122.7(10)	N(2)–C(7)–C(8)	111.2(9)
C(6)–C(7)–C(8)	126.0(11)	C(7)–C(8)–C(9)	105.5(10)
C(8)–C(9)–C(10)	107.5(10)	N(2)–C(10)–C(9)	111.9(10)
N(2)–C(10)–O(1A)	123.8(10)	C(9)–C(10)–O(1A)	124.3(10)
Fe–C(19)–N(3)	177.4(11)		

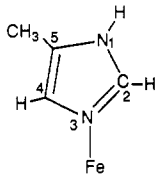

B

conditions. Consequently, the identification of paramagnetically shift resonances in trace C is facilitated. Under these conditions, where a slight excess of 4-MeIm is present, it is apparent that the sample has been converted into the low-spin complex $[(OEOP)Fe^{III}(5\text{-MeIm})_2]^{2+}$. The resonance assignments given in Figure 7 are readily made on the basis of intensity, comparison with the data described above for $(OEOP)Fe^{III}(CN)_2$, and comparison with spectra obtained for $[PFe^{III}(5\text{-MeIm})_2]^{+}$.[24] Thus, on the basis of their chemical shifts, the resonances of the axial 5-MeIm ligands (5-Me, and broad 2-H and 4-H) are readily apparent. The set of four equally intense resonances at 13.5, 12.0, 8.5, and 2.0 ppm are assigned to the methylene protons. The three resonance at 0.0, −1.5, and −2.0 ppm are assigned to the methyl protons. The resonance at 9 ppm is due to the two equivalent meso protons, and the resonances at 3.8 and 8.8 ppm are due either to the remaining meso proton (m′) or to the 1-H

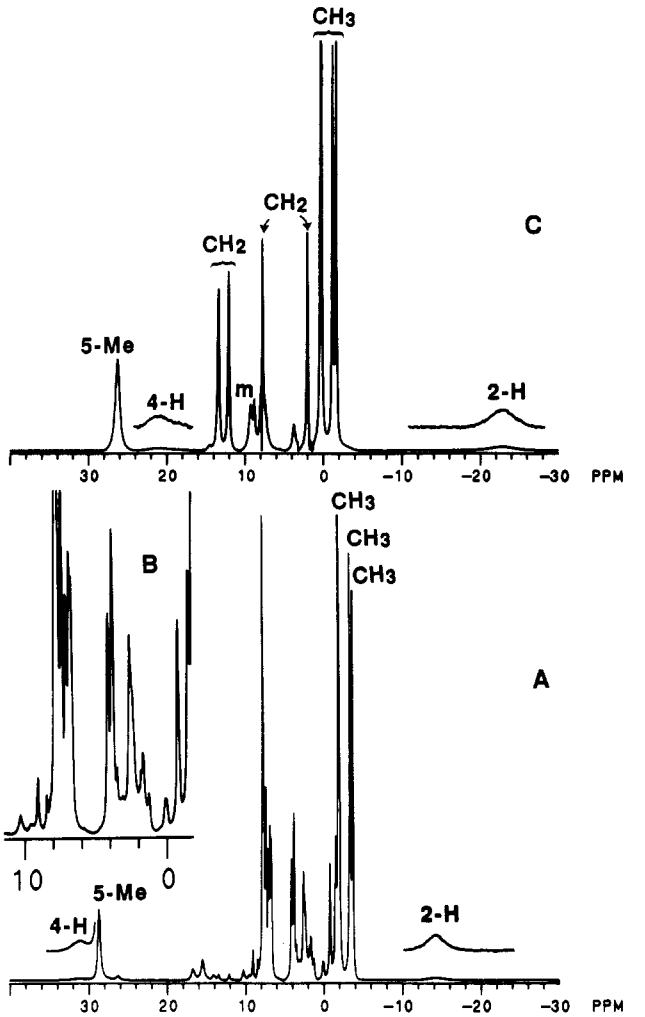

Figure 7. 300-MHz ^1H NMR spectra of a chloroform-*d* solution of $(OEOP)Fe^{III}Cl_2$ at −60 °C: (A) spectrum after addition of 1 equiv of 4-MeIm; (B) an expansion of the +10 to −2 ppm region of the spectrum shown in (A); (C) spectrum after addition of 2.3 equiv of 4-MeIm.

resonance of 5-MeIm. Definitive assignment between these two possibilities cannot be made with the existing data.

When only 1 equiv of 4-MeIm has been added to $(OEOP)Fe^{III}Cl_2$, it is apparent that a second, low-spin species is present. This is evident when traces A and C of Figure 7 are compared. Trace A shows a separate set of resonances. The major differences that are readily identified are the location of the resonances of the axial ligands, the occurrence of methyl resonances in trace A that are upfield of those in trace C, and the virtual absence of the four methylene resonances of $[(OEOP)Fe^{III}(5\text{-MeIm})_2]^{2+}$ in trace A. We can confidently identify the species responsible for these differences as the low-spin complex $[(OEOP)Fe^{III}Cl(5\text{-MeIm})]^{+}$. The ratio of intensity of the 5-Me resonance to the intensity of the OEOP methyl resonances establishes the stoichiometry of 5-MeIm binding to $(OEOP)Fe^{III}$ as 1:1. The methylene and meso resonances of this complex occur in the complex region between −2 and +8 ppm. Since the two axial ligands are inequivalent, eight methylene resonances are expected and indeed eight lines can be discerned within the −2 to +8 ppm region as shown in trace B.

On warming, the spectrum shown in trace C of Figure 7 undergoes the usual changes expected for a paramagnetic complex. Thus, the complex $[(OEOP)Fe^{III}(5\text{-MeIm})_2]^{2+}$ appears to remain intact upon warming.

Similar data have been obtained which indicate that methyl isocyanide and pyridine also react with $(OEOP)Fe^{III}Cl_2$ to form low-spin species. In all cases, however, it is important that an excess of these axial ligands be avoided. In the presence of excess

pyridine, for example, (OEOP)$Fe^{III}Cl_2$ is reduced and $[(OEOP)Fe^{II}(py)_2]^+$ is formed.[18] Similarly, addition of excess cyanide ion or 4-MeIm results in the conversion of (OEOP)$Fe^{III}Cl_2$ into diamagnetic Fe(II) complexes.

Discussion

The present study clearly establishes the existence of low-spin, six-coordinate iron(III) complexes of octaethyloxoporphyrin. These are formed with the same group of strong-field ligands that lead to the formation of low-spin, six-coordinate iron(III) porphyrin complexes. These ligand-exchange reactions occur without alteration of the oxoporphyrin ligand. On the other hand, $[(OEOP)Fe^{II}(py)_2]^+$ undergoes ring opening when treated with hydroxide ion,[12] and it also reacts with ammonia to form an azaporphyrin.[25,26] The porphyrins and oxoporphyrins form closely related iron complexes with similar responses to changes in axial ligation. This point is also emphasized by the fact that pyridine and cyanide ion are capable of reducing both iron(III) porphyrin[27,28] and oxoporphyrin complexes to the iron(II) forms.

Although the crystal structure of (OEOP)$Fe^{III}(CN)_2$ is disordered, the combination of X-ray and ^{1}H NMR studies makes it clear that the complex contains the nearly planar oxoporphyrin core and has idealized C_{2v} symmetry in solution. A previous structural study of the zinc complex of the oxoporphyrin obtained by ring closure of biliverdin showed that this macrocycle, like that in (OEOP)$Fe^{III}(CN)_2$, is planar.[29] Solid-state disorder of core-modified porphyrins, such as the oxoporphyrins, has been encountered in a variety of structural studies.[18] Since the periphery of (OEOP)$Fe^{III}(CN)_2$ is made up of eight nearly identical ethyl groups, the external shape of the molecule is barely perturbed by the substitution of an oxo function for a methine group.

With the thorough characterization of the structural aspects and spectroscopic features of the verdoheme derivatives described in this paper and in ref 18, the stage is now set for a more careful examination of the reactions that lead to the degradation of heme via the coupled oxidation process. Studies relevant to the mechanism of this chain of events are in progress.

Experimental Section

Preparation of Compounds. (OEOP)$Fe^{III}Cl_2$ was prepared as described previously.[18]

(OEOP)$Fe^{III}(CN)_2$. A sample of 81 mg (0.15 mmol) of bis(triphenylphosphine)nitrogen(1+) cyanide was added to a green solution of 20 mg (0.033 mmol) of (OEOP)$Fe^{III}Cl_2$ that was dissolved in 5 mL of dichloromethane. After 2 min of standing, diethyl ether was slowly added to the solution to precipitate the product as dark red crystals. These were collected by filtration, washed with two 10-mL portions of water and four 5-mL portions of methanol, and vacuum-dried to give 13.8 mg (75%) of the product. Purification was achieved by dissolving the product in dichloromethane, filtering, and reprecipitating the product with diethyl ether. Trace A of Figure 1 shows the absorption spectrum while Figure 2 shows the ^{1}H NMR spectrum.

Table III. Crystallographic Data for (OEOP)$Fe^{III}(CN)_2 \cdot 1.6CH_2Cl_2$

$C_{38.6}H_{46.2}Cl_{3.2}FeN_6O$	fw = 779.5
a = 12.750(4) Å	$P2_1/c$, monoclinic
b = 8.069(3) Å	T = 130 K
c = 19.728(8) Å	λ(Mo Kα) = 0.710 73 Å
β = 99.67(3)°	d_{calcd} = 1.294 Mg/m^3
V = 2000.9(12)	transm factors = 0.86–0.92
Z = 2	μ = 0.628 mm^{-1}
$R(F)^a$ = 0.076	$R_w(F)^a$ = 0.078

^{a} $R = \sum||F_o| - |F_c||/\sum|F_o|$; $R_w = \sum||F_o| - |F_c||w^{1/2}/\sum|F_o|w^{1/2}$; $w^{-1} = \sigma^2|F| + 0.0022F^2$.

Addition of 4-MeIm to (OEOP)$Fe^{III}Cl_2$. A 2 mM solution of (OEOP)$Fe^{III}Cl_2$ in chloroform-*d* was prepared and cooled to –60 °C. A 1.0 M solution of 4-MeIm in chloroform-*d* was introduced stepwise into the sample by means of a hypodermic syringe. The ^{1}H NMR spectral data are shown in Figure 7.

X-ray Data Collection for OEOP$Fe^{III}(CN)_2$. A dark red block was obtained by direct diffusion of diethyl ether into a solution of the complex in dichloromethane. A suitable crystal was coated with a light hydrocarbon oil and mounted in the 130 K dinitrogen stream of a Siemens R3m/V diffractometer that was equipped with a low-temperature device. Two check reflections showed only random (>2%) variation during data collection. The data were corrected for Lorentz and polarization effects. Crystal data are given in Table III.

Solution and Refinement of the Structure. Calculations were performed on a DEC VAX station 3200 with the programs of SHELXTL Plus v. 4.0. Scattering factors for neutral atoms and corrections for anomalous dispersion were taken from a standard source.[30] An absorption correction was applied to the structure.[31] The solution of the structure was obtained by a Patterson synthesis. During the last stages of refinement, the iron atom was assigned anisotropic thermal parameters. Hydrogen atoms were located on a difference map and refined at ideal geometries for subsequent cycles of least-squares refinement. The largest peak on the final difference map, 0.86 e Å^{-3}, is 0.9 Å from Cl(1) and is a likely artifact of the dichloromethane disorder.

Instrumentation. ^{1}H NMR spectra were recorded on a General Electric QE-300 FT NMR spectrometer operating in the quadrature mode (^{1}H frequency is 300 MHz). The spectra were collected over a 50-kHz bandwidth with 16K data points and a 5-μs 45° pulse. For a typical spectrum, between 1000 and 5000 transients were accumulated with a 50-ms delay time. The signal to noise ratio was improved by apodization of the free induction decay. The M-COSY data were obtained as described previously.[20] Electronic spectra were obtained using a Hewlett Packard diode array spectrometer. ESR spectra were obtained using a Bruker spectrometer. The magnetic moment was measured by the Evans technique.[32]

Acknowledgment. We thank the National Institutes of Health (Grant GM-26226) for financial support.

Supplementary Material Available: Tables of all bond lengths, bond angles, anisotropic thermal parameters, hydrogen atom positions and data collection parameters for (OEOP)$Fe^{III}(CN)_2 \cdot 1.6CH_2Cl_2$ (7 pages). Ordering information is given on any current masthead page.

(25) Lemberg, R. *Aust. J. Exp. Biol. Med. Sci.* **1943**, *21*, 239.
(26) Balch, A. L.; Olmstead, M. M.; Safari, N. *Inorg. Chem.* **1993**, *32*, 291.
(27) Del Gaudio, J.; LaMar, G. N. *J. Am. Chem. Soc.* **1978**, *100*, 1112.
(28) LaMar, G. N.; Del Gaudio, J. *Adv. Chem. Ser.* **1977**, *162*, 207.
(29) Fuhrhop, J.-H,: Kruger, P.; Sheldrick, W. S. *Justus Liebigs Ann. Chem.* **1977**, 339.
(30) *International Tables for X-ray Crystallography*; Kynoch Press: Birmingham, England, 1974; Vol. 4.
(31) The method obtains an empirical absorption tensor from an expression relating F_o and F_c: Moezzi, B. Ph.D. Thesis, University of California, Davis, 1987.
(32) Evans, D. F. *J. Chem. Soc.* **1959**, 2003.